Whee Kuk Kim

Department of Control & Instrumentation Engineering
Korea University
Seochangdong, Chochiwon, Yongi,
Chungnam, 339-800, Korea
wheekuk@tiger.korea.ac.kr

Yong Kyu Byun

Nano System Laboratory
Samsung Advanced Institute of Technology
P.O. Box 111, Suwon 440-600, Korea
ykbyun@sait.samsung.co.kr

Hyung Suck Cho

Department of Mechanical Engineering
Korea Advanced Institute of Science and Technology
373-1 Kusongdong,Yusonggu,Taejon, 305-701, Korea
hscho@lca.kaist.ac.kr

Closed-Form Forward-Position Solution for a 6-DoF 3-PPSP Parallel Mechanism and Its Implementation

Abstract

Closed-form forward/reverse position solutions for a 6-degree-of-freedom (DoF) parallel mechanism that has some type of nonsymmetric geometry are derived in this study. Particularly, the derived forward-position analysis is applicable to the mechanisms in which three passive joints are constrained to move parallel to the moving plate. Its kinematic and dynamic characteristics are investigated via isotropic index of the Jacobian matrix and isotropic index of the output effective inertia matrix, respectively. From this investigation, it is found that the mechanism has fairly uniform kinematic/dynamic characteristics throughout its workspace. To examine the effectiveness of the proposed 3-PPSP-type mechanism, a prototype is designed, implemented, and tested experimentally under various operating conditions. A simple PID controller is applied to the system, and its joint positions are servo-controlled. The controlled system showed a good trajectory performance. Noting that a more advanced controller requiring a forward- and/or reverse-position solution can be applied to the system in real time, it can be contended that the manipulator is a candidate for the high-precision manipulator.

KEY WORDS—parallel manipulator, closed-form solution, 6-DoF, 3-PPSP

The International Journal of Robotics Research
Vol. 20, No. 1, January 2001, pp. 85-99,

1. Introduction

Parallel mechanism consists of several serial subchains that are constrained to each other. Therefore, it is known that due to its intrinsic kinematic constraints, the parallel mechanism has higher stiffness and payload capability and is more effective in tasks requiring high precision compared with the other types of mechanisms. On the other hand, it is known that much higher complexities are involved in analyzing the mechanism. Particularly, the forward-position analysis of the parallel mechanism is quite complicated compared to the one for the serial mechanism, while the reverse position analysis of the parallel mechanism can be obtained with relative easiness compared to the forward-position analysis. Therefore, to utilize advantageous characteristics of the parallel mechanisms without being degradated due to its analytical complexity, many efforts either to design the parallel mechanism that has closed-form forward-position solution or to find its closed-form forward-position solution have been made in literature.

Behi (1988) proposed a parallel manipulator consisting of 3-PRPS serial subchains and showed that three independent forward-kinematics solutions can be obtained from three nonlinear equations with three unknowns through numerical analysis. Kohli and Lee (1988) proposed a mechanism consisting of rotary-linear (R-L) drive mechanisms and showed that 32 forward-kinematics solutions can be obtained from a 16th-order polynomial equation. Hudgens and Tesar (1991)

proposed a micro-manipulator consisting a four-bar mechanism with a high reduction ratio applicable to a robotic wrist and performed a forward-kinematics analysis similar to the Stewart platform mechanism. Cleary and Brooks (1993) proposed a parallel manipulator consisting of all revolute joints and showed that the convergence speed for three nonlinear equations with three unknowns approaches a real-time solution using numerical analysis. Alizade and Tagiyev (1994) devised a parallel manipulator with a drive mechanism composed of three SP links mounted on moving sliders, allowing pure rotation in the vertical direction. They demonstrated its advantages on the workspace and solved for 11 forward-kinematics solutions from nine nonlinear equations. Tsai and Tahmasobi (1993) developed a 2-DoF drive mechanism in the form of a pantographic linkage. They applied this to a hybrid serial/parallel manipulator mechanism that can be described by nine 8th-order polynomials with nine unknowns, resulting in a maximum of 16 forward-kinematics solutions.

Until now, there has been only a small number of the proposed parallel mechanisms that have been known in the literature to have closed-form forward-position solutions. In fact, when the parallel mechanism does not have the closed-form solution of forward-position analysis, it could be found by a numerical method. As an alternative, a method of attaching extra sensors to the mechanism is suggested by Merlet (1993). However, due to spatial limitations such as mechanical interference, inadequate locations of sensor attachment, and accumulated sensing errors, the method is not so effective to be used frequently.

In a previous study, Byun and Cho (1997) proposed the 6-DoF 3-PPSP-type parallel mechanism. Its closed-form forward-position solution is described, and its workspace analysis to examine motion capability is performed. However, the closed-form solution is valid only to the mechanism that has a symmetric system parameter. In general, in real hardware implementation, the mechanism cannot maintain the symmetric system parameters perfectly, due to its tolerances or other design/manufacturing errors.

Therefore, in this study, we derived a closed-form forward-position solution for the 3-PPSP-type 6-DoF parallel mechanism, which may not be symmetric. More specifically, the solution is valid to the mechanisms that are actuated by the first two prismatic joints of each of three serial subchains and that meet the following condition: the three passive prismatic joints attached to the moving plate are constrained to move parallel to the moving platform. The other system parameters of the mechanism do not need to be symmetric.

It can be noted that the mechanism may not be adequate in tasks subject to high payloads, since when high output force is applied to the mechanism in the direction perpendicular to ones of those three passive joint axes, the mechanism may be jammed due to increased friction forces. However, the mechanism is expected to exert an excellent performance, particularly when it is applied to tasks requiring high precision but not subject to high payloads. Therefore, a prototype manipulator is implemented and tested to examine its performance (Byun et al. 1998).

This paper is summarized as follows. After brief description of the 3-PPSP parallel mechanism, closed-form forward/reverse-position solutions of the mechanism are derived. Then, its kinematic and dynamic characteristics are investigated via the isotropic index of the Jacobian matrix and the output effective inertial matrix, respectively. Last, a prototype manipulator system is designed and implemented, the joint position servo-controller is applied to the system, and its performance is tested. Then, a conclusion is given based on these analyses and experiments.

2. Position Analysis of the Mechanism

The 6-DoF 3-PPSP parallel manipulator illustrated in Figure 1 consists of a platform and a base that are connected by three serial subchains. Each of three 6-DoF serial subchains is composed of two active prismatic joints (PP) joined perpendicularly, a spherical joint (S), and a passive prismatic joint (P) on the platform. Particularly, note that the passive prismatic joint of each of three subchains is constrained to move parallel to the platform.

The mobility of the mechanism is found to be 6 using the Grubler's mobility (M) equation as

$$M = d(n - g - 1) + \sum_{j=1}^{g} f_j, \tag{1}$$

where d, n, g, and f_j represent the order of motion space of the system, number of links including the base, number of joints, and number of degrees of freedom for the jth joint, respectively.

As seen in Figure 1, there are 11 links ($n = 11$) and 12 joints ($g = 12$) in the device. Note that d is 6 since the mechanism is a spatial device. Substituting these values into eq. (1), the resulting mobility of the parallel manipulator is found to be 6.

2.1. Description of the Mechanism

For convenience of presentation, consider the mechanism of which three axes of three passive prismatic joints have a common intersection point as shown in Figure 2. Frames $(\boldsymbol{x}_b, \boldsymbol{y}_b, \boldsymbol{z}_b)$ and $(\boldsymbol{x}_p, \boldsymbol{y}_p, \boldsymbol{z}_p)$ represent a base frame and an output frame with an origin fixed at a point where the axes of three passive prismatic joints intersect, respectively.

Let us denote the input vector of the mechanism as

$$\boldsymbol{d} = \begin{bmatrix} {}_1d_1 & {}_1d_2 & {}_2d_1 & {}_2d_2 & {}_3d_1 & {}_3d_2 \end{bmatrix}^T, \tag{2}$$

where ${}_id_j$ denotes the jth prismatic joint variable of ith serial subchain. And denote the output position vector of the

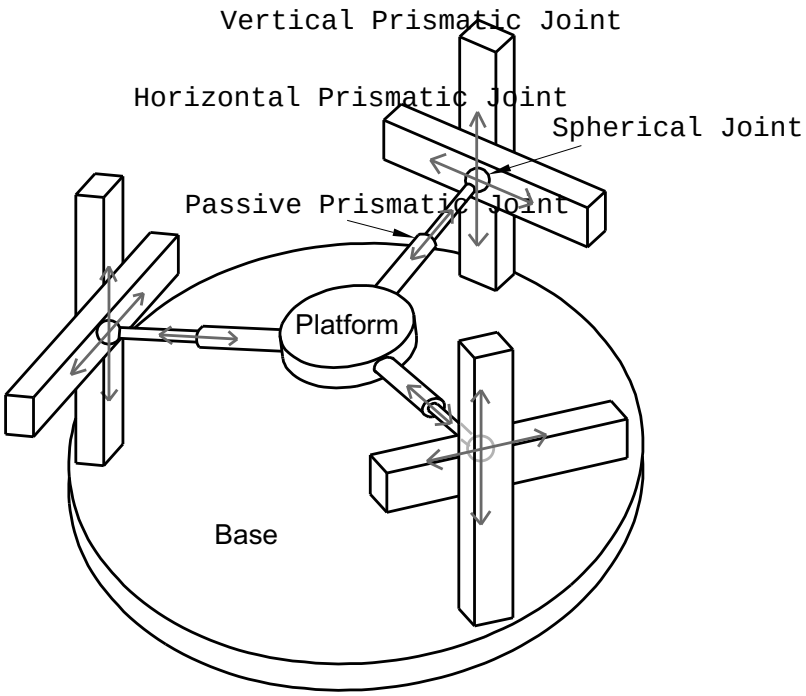

Fig. 1. The 6-DoF 3-PPSP parallel mechanism.

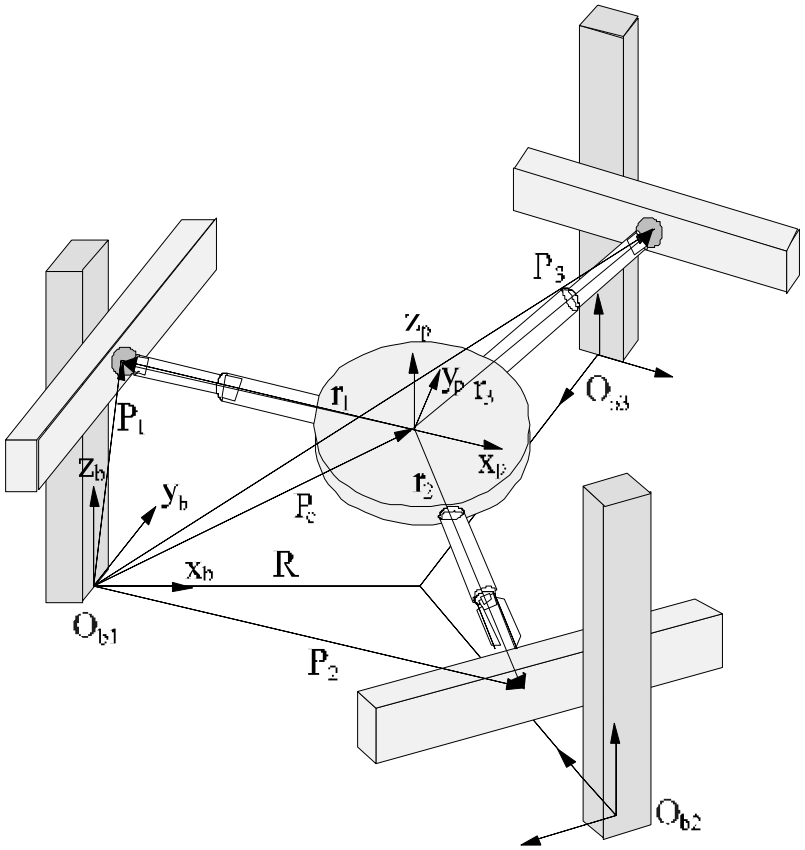

Fig. 2. Schematic diagram for kinematics.

mechanism as $\boldsymbol{P}_c = [xyz]^T$. It can be noted that the output position is the common intersection point of those three passive prismatic joint axes. And let the output orientation of the mechanism be represented by the following x-y-z Euler angles

$$\begin{aligned}\left[R_b^p\right] &= [Rot(\boldsymbol{x}, \alpha)]\,[Rot(\boldsymbol{y}, \beta)][Rot(\boldsymbol{z}, \gamma)] \\ &= \begin{bmatrix} C_\beta C_\gamma & -C_\beta S_\gamma & S_\beta \\ S_\alpha S_\beta C_\gamma + C_\alpha S_\gamma & -S_\alpha S_\beta S_\gamma + C_\alpha C_\gamma & -S_\alpha C_\beta \\ -C_\alpha S_\beta C_\gamma + S_\alpha S_\gamma & C_\alpha S_\beta S_\gamma + S_\alpha C_\gamma & C_\alpha C_\beta \end{bmatrix}. \end{aligned} \tag{3}$$

This matrix represents the direction cosine of the output frame unit vectors with respect to the base frame unit vectors. For simplicity, denote its elements as

$$\left[R_b^p\right] = \begin{bmatrix} x_{p1} & y_{p1} & z_{p1} \\ x_{p2} & y_{p2} & z_{p2} \\ x_{p3} & y_{p3} & z_{p3} \end{bmatrix}. \tag{4}$$

Therefore, the output position vector of the mechanism is written as

$$\boldsymbol{E}_o = \begin{bmatrix} x & y & z & \alpha & \beta & \gamma \end{bmatrix}^T. \tag{5}$$

Geometric description of the whole mechanism can be represented by one of the subchains of the parallel manipulator, and Denavit-Hartenberg (DH) link parameters for a PPSP serial subchain in Figure 3 are summarized in Table 1. Note that twist angles (0, 90, and 90 deg) and revolute joint variables ($\theta_3, \theta_4, \theta_5$) are used to denote the ball and socket joint in Table 1.

2.2. Forward-Position Analysis

Forward-position analysis finds the position/orientation of the platform of the mechanism when the input joint variables are specified. In this section, a closed-form forward-position solution of the 3-PPSP-type 6-DoF parallel mechanism is derived. The closed-form solution is valid to the mechanism satisfying the following condition: three passive prismatic joint axes of the mechanism are placed on the planes parallel to each other. In the following analysis, for convenience of presentation, it is assumed that three passive prismatic joint axes of the mechanism are placed on the same plane. Two active prismatic joints of each of three serial subchains can be placed arbitrarily. Assuming that displacements of two active prismatic joints of each serial subchain are measured, the position vector from the origin of the base frame to the point P_i (for $i = 1, 2, 3$) representing the center position of three spherical joints, can be found as

$$\boldsymbol{P}_i = \boldsymbol{P}_{bi} + {}_i d_1\ {}_i\boldsymbol{z}_1 + {}_i d_2\ {}_i\boldsymbol{z}_2, \tag{6}$$

where $\boldsymbol{P}_{bi}$ represents the absolute position vector from the origin of the reference frame to the origin of the local base frame of the ith serial subchain,

$${}_i\boldsymbol{z}_j = \left[{}_i R_b^o\right]\left[{}_i R_b^j\right]\begin{bmatrix}0\\0\\1\end{bmatrix}, \tag{7}$$

$$\boldsymbol{P}_i = (P_{ix}, P_{iy}, P_{iz})^T, \tag{8}$$

and $[{}_i R_b^o]$ and $[{}_i R_b^j]$ represent a rotational matrix from the base frame of the mechanism to the local base frame and the jth local frame of the ith serial subchain, respectively. Thus, the subsystem including three passive prismatic joints and a moving plate can be simplified as in Figure 4.

Using Figure 4, the closed form of the forward-position solution is found in the following three steps:

Step (i) find the displacements of three passive prismatic joints ($\boldsymbol{r}_1, \boldsymbol{r}_2, \boldsymbol{r}_3$),

Step (ii) find the position of the platform of the system (x, y, z),

Step (iii) find the orientation of the platform of the system (α, β, γ).

2.2.1. Displacements of Three Passive Prismatic Joints ($\boldsymbol{r}_1, \boldsymbol{r}_2, \boldsymbol{r}_3$)

Under the above assumption, as shown in Figure 4, the triangle that is formed by connecting three points P_1, P_2, and P_3 is aligned with the platform on which three passive prismatic joints are constrained to move. Noting that three axes of passive prismatic joints are on the same plane, they intersect at points of C_{12}, C_{23}, and C_{31}, respectively. Now, denote the distances between C_{12} and C_{23}, between C_{23} and C_{31}, and between C_{31} and C_{12} as u, v, and w, respectively. These three values represent fixed offsets for the implemented system. Denote the angles $\angle P_1C_{12}P_2$, $\angle P_2C_{23}P_3$, and $\angle P_3C_{31}P_1$ as ψ_{12}, ψ_{23}, and ψ_{31}, respectively. And denote the position vectors from point C_{31} to P_1, from C_{12} to P_2, and from C_{23} to P_3 and its corresponding magnitudes as $\boldsymbol{r}_1, \boldsymbol{r}_2, \boldsymbol{r}_3$, and r_1, r_2, r_3, respectively. Furthermore, denote the angles $\angle C_{31}P_1P_2$ and $\angle C_{31}P_1P_3$ as θ_{1r} and θ_{1l}.

The center positions of the three spherical joints (P_1, P_2, P_3) could be found as in (6). Also, the distances between those three points P_{12}, P_{31}, and P_{23} can easily be computed. Note that from Figure 4, it can be easily seen that

$$\theta_{1l} = \theta_1 - \theta_{1r}, \tag{9}$$

$$\theta_{2l} = \pi - \psi_{12} - \theta_{1r}, \tag{10}$$

$$\theta_{3r} = \pi - \psi_{31} - \theta_{1l} = \pi - \psi_{31} - \theta_1 + \theta_{1r}. \tag{11}$$

Using the law of cosine, an angle θ_1, which represents an angle $\angle P_2P_1P_3$ can be found as

$$\theta_1 = a\cos\frac{P_{31}^2 + P_{12}^2 - P_{23}^2}{2P_{12}P_{31}}. \tag{12}$$

Table 1. Denavit-Hartenberg (DH) Link Parameters of PPSP Serial Subchain

Link #n	α_{n-1}	a_{n-1}	d_n	θ_n
Offset	${}_1r_b = 0°$, ${}_2r_b = 120°$, ${}_3r_b = 240°$, $R = 0.195$m			${}_i\gamma_b$
1	0	0	d_1	0
2	−90	0	d_2	0
3	0	0	0	θ_3
4	90	0	0	θ_4
5	90	0	0	θ_5
6	0	0	d_6	0
Platform	−90	0	0	${}_i\gamma_p$
Offset	${}_1r_p = 270°$, ${}_2r_p = 30°$, ${}_3r_p = 150°$			

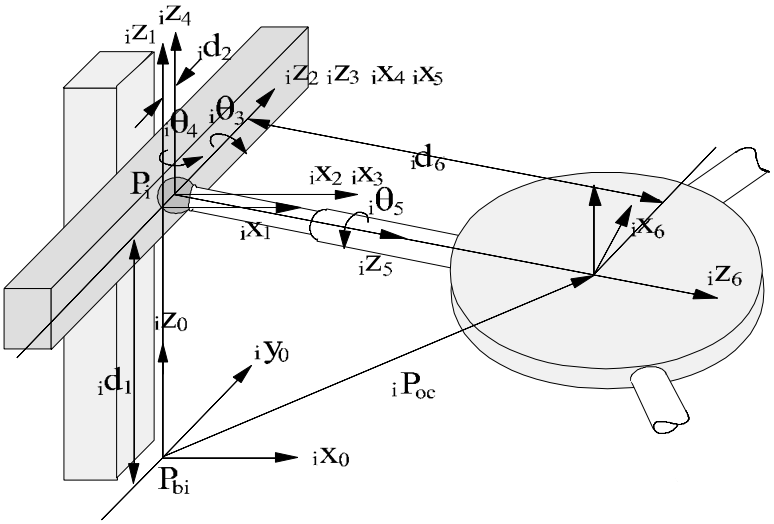

Fig. 3. Kinematic model of a PPSP serial subchain.

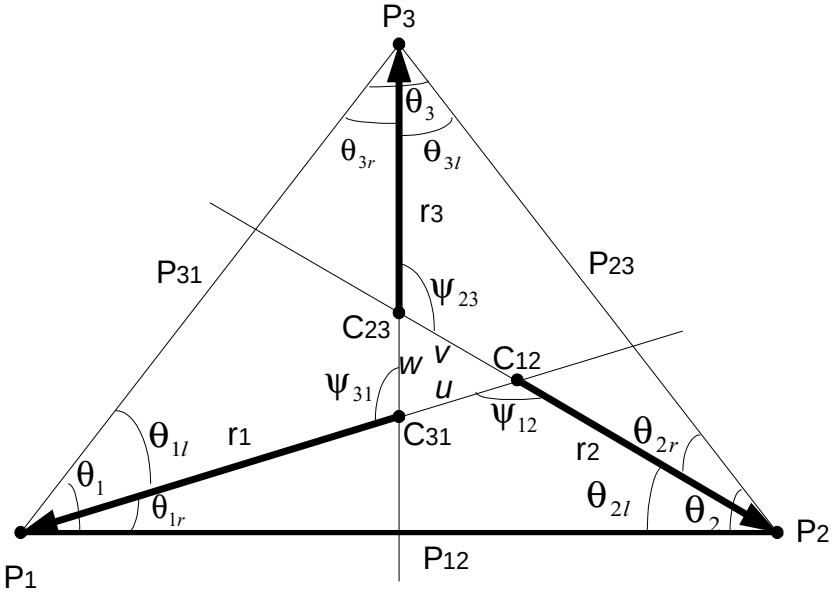

Fig. 4. Kinematic model for the subparts including three passive joints and a moving plate.

Using the law of sine on $\triangle P_1P_2C_{12}$, the following relations hold:

$$\frac{r_1+u}{\sin(180^\circ-\psi_{12}-\theta_{1r})}=\frac{P_{12}}{s\psi_{12}}, \tag{13}$$

$$\frac{r_1}{\sin(180^\circ-\psi_{31}-\theta_1-\theta_{1r})}=\frac{P_{31}}{s\psi_{31}}. \tag{14}$$

Similarly, applying the law of sine on $\triangle P_3P_1C_{31}$ and $\triangle P_1P_2C_{12}$, respectively, yields

$$\frac{P_{31}}{s\psi_{31}}=\frac{r_3+w}{s\theta_{1l}}, \tag{15}$$

$$\frac{r_2}{s\theta_{1r}}=\frac{P_{12}}{s\psi_{12}}. \tag{16}$$

By removing r_1 from (13) and (14), we have

$$A\cos\theta_{1r}+B\sin\theta_{1r}-C=0, \tag{17}$$

where

$$A=P_{12}-\frac{P_{31}}{s\psi_{31}}\sin(\psi_{31}+\theta_1), \tag{18}$$

$$B=\frac{P_{12}}{s\psi_{12}}c\psi_{12}-\frac{P_{31}}{s\psi_{31}}\cos(\psi_{31}+\theta_1), \tag{19}$$

$$C=u. \tag{20}$$

Solving for θ_{1r} yields

$$\theta_{1r}=A\tan 2(B,A)\pm A\tan 2\left(\sqrt{A^2+B^2-C^2},C\right). \tag{21}$$

In eq. (21), the solution of θ_{1r} is 2, but it can be easily seen that the solution inside the following boundary, $0\le\theta_{1r}\le\theta_1$, is the desired solution. Substituting the obtained θ_{1r} into (14), (15), and (16) yields r_1, r_2, r_3, respectively, as follows:

$$r_1=\frac{P_{31}}{s\psi_{31}}\sin(\psi_{31}-\theta_1-\theta_{1r}), \tag{22}$$

$$r_2=\frac{s\theta_{1r}}{s\psi_{12}}P_{12}, \tag{23}$$

$$r_3=\frac{s\theta_{1l}}{s\psi_{31}}P_{31}-w. \tag{24}$$

2.2.2. Position of the Platform of the System (x, y, z)

For convenience of presentation, from now on, it is further assumed that the three axes of passive prismatic joints intersect at a common point and let the point be the output position of interest of the mechanism, P_c as shown in Figure 2. Note that with minor modification, the following procedure could be applied to the case of not having common intersection point in Section 2.2.1. For the case of having a common intersection point, the values of three fixed offsets become zero ($u=v=w=0$). Thus, the position vectors from the point P_c to $P_i(i=1,2)$, $\boldsymbol{r}_1$ and $\boldsymbol{r}_2$, can be expressed as

$$\boldsymbol{r}_1=\boldsymbol{P}_1-\boldsymbol{P}_c, \tag{25}$$

$$\boldsymbol{r}_2=\boldsymbol{P}_2-\boldsymbol{P}_c. \tag{26}$$

From the fact that the vector $\boldsymbol{r}_1\times\boldsymbol{r}_2$ parallels the unit vector of the top frame, $\boldsymbol{z}_p$, the following equation can be written

$$\frac{(\boldsymbol{r}_1\times\boldsymbol{r}_2)_x}{(\boldsymbol{r}_1\times\boldsymbol{r}_2)_z}=\frac{z_{p1}}{z_{p3}}, \tag{27}$$

where $\boldsymbol{r}_1\times\boldsymbol{r}_2$ is found from eqs. (25) and (26),

$$\boldsymbol{r}_1\times\boldsymbol{r}_2=\begin{bmatrix}(P_{1z}-P_{2z})y+(P_{2y}-P_{1y})z+P_{1y}P_{2z}-P_{1z}P_{2y}\\(P_{2z}-P_{1z})x+(P_{1x}-P_{2x})z+P_{1z}P_{2x}-P_{1x}P_{2z}\\(P_{1y}-P_{2y})x+(P_{2x}-P_{1x})y+P_{1x}P_{2y}-P_{1y}P_{2x}\end{bmatrix}. \tag{28}$$

Eq. (27) can be arranged with respect to x, y, z as below:

$$k_1x+k_2y+k_3z+k_4=0, \tag{29}$$

where

$$k_1=\frac{z_{p1}}{z_{p3}}(P_{1y}-P_{2y}), \tag{30}$$

$$k_2=\frac{z_{p1}}{z_{p3}}(P_{2x}-P_{1x})-(P_{1z}-P_{2z}), \tag{31}$$

$$k_3=-(P_{2y}-P_{1y}), \tag{32}$$

$$k_4=\frac{z_1}{z_{p3}}(P_{1x}P_{2y}-P_{1y}P_{2x})-(P_{1y}P_{2z}-P_{1z}P_{2y}). \tag{33}$$

Inner product of $-\boldsymbol{r}_1$ and $(\boldsymbol{P}_2-\boldsymbol{P}_1)$, and inner product of $-\boldsymbol{r}_1$ and $(\boldsymbol{P}_3-\boldsymbol{P}_1)$ can be expressed, respectively, as

$$-\boldsymbol{r}_1\cdot(\boldsymbol{P}_2-\boldsymbol{P}_1)=r_1P_{12}c\theta_{1r}, \tag{34}$$

$$-\boldsymbol{r}_1\cdot(\boldsymbol{P}_3-\boldsymbol{P}_1)=r_1P_{13}c\theta_{1l}, \tag{35}$$

and they can be written as follows:

$$(P_{2x}-P_{1x})x+(P_{2y}-P_{1y})y+(P_{2z}-P_{1z})z+w_1=0, \tag{36}$$

$$(P_{3x}-P_{1x})x+(P_{3y}-P_{1y})y+(P_{3z}-P_{1z})z+w_2=0, \tag{37}$$

where

$$\begin{aligned}w_1=&-P_{12}r_1c\theta_{1r}-(P_{2x}-P_{1x})P_{1x}\\&-(P_{2y}-P_{1y})P_{1y}-(P_{2z}-P_{1z})P_{1z},\end{aligned} \tag{38}$$

$$\begin{aligned}w_2=&-P_{13}r_1c\theta_{1l}-(P_{3x}-P_{1x})P_{1x}\\&-(P_{3y}-P_{1y})P_{1y}-(P_{3z}-P_{1z})P_{1z}.\end{aligned} \tag{39}$$

From eqs. (29), (36), and (37), x, y, and z can be found as follows:

$$\begin{bmatrix} x \\ y \\ z \end{bmatrix} = \begin{bmatrix} P_{2x} - P_{1x} & P_{2y} - P_{1y} & P_{2z} - P_{1z} \\ P_{3x} - P_{1x} & P_{3y} - P_{1y} & P_{3z} - P_{1z} \\ k_1 & k_2 & k_3 \end{bmatrix}^{-1} \begin{bmatrix} -w_1 \\ -w_2 \\ -k_4 \end{bmatrix}. \tag{40}$$

2.2.3. Orientation of the Platform of the System (α, β, γ)

The vector perpendicular to the platform in upward direction can be found as

$$\boldsymbol{Z}_p = (\boldsymbol{P}_2 - \boldsymbol{P}_1) \times (\boldsymbol{P}_3 - \boldsymbol{P}_1) = \begin{bmatrix} Z_{p1} & Z_{p2} & Z_{p3} \end{bmatrix}^T, \tag{41}$$

where

$$\begin{aligned} Z_{p1} = {} & -P_{1z}P_{2y} + P_{1y}P_{2z} + P_{1z}P_{3y} - P_{2x}P_{3y} \\ & - P_{1y}P_{3x} + P_{2y}P_{3z}, \end{aligned} \tag{42}$$

$$\begin{aligned} Z_{p2} = {} & P_{1z}P_{2x} - P_{1x}P_{2x} - P_{1z}P_{3x} + P_{2z}P_{3x} \\ & + P_{1x}P_{3z} - P_{2x}P_{3z}, \end{aligned} \tag{43}$$

$$\begin{aligned} Z_{p3} = {} & -P_{1y}P_{2x} + P_{1x}P_{2y} + P_{1y}P_{3x} - P_{2y}P_{3x} \\ & - P_{1x}P_{3y} + P_{2x}P_{3y}. \end{aligned} \tag{44}$$

Furthermore, $\boldsymbol{z}_p$ can be expressed from eq. (41) as

$$\boldsymbol{z}_p = \frac{\boldsymbol{Z}_p}{\|\boldsymbol{Z}_p\|} = \begin{bmatrix} s\beta \\ -s\alpha c\beta \\ c\alpha c\beta \end{bmatrix}, \tag{45}$$

and from this equation, α and β can be found as follows:

$$\alpha = a\tan 2(-z_{p2}, z_{p3}), \tag{46}$$

$$\beta = a\tan 2\left(z_{p1}, \sqrt{z_{p2}^2 + z_{p3}^3}\right). \tag{47}$$

Also, using the following relation,

$$\boldsymbol{r}_1 = -r_1\boldsymbol{x}_p = \boldsymbol{P}_1 - \boldsymbol{R}_t, \tag{48}$$

the rotational output displacement γ can be found as below:

$$\gamma = a\tan 2(c\alpha(P_{1y} - y) + s\alpha(P_{1z} - z), (P_{1x} - x)/c\beta). \tag{49}$$

2.3. Inverse Position Analysis

Denote $[{}_i R_o^6]$ and ${}_i\boldsymbol{P}_{oc}$ as a rotational matrix and the local position vector from the origin of the base frame of the ith serial subchain to the origin of the 6th local frame, respectively. From Table 1, the homogeneous transformation matrix from the base frame to the output frame can be written as

$${}_i T_o^6 = {}_i T_o^1 {}_i T_1^2 {}_i T_2^3 {}_i T_3^4 {}_i T_4^5 {}_i T_5^6. \tag{50}$$

From eq. (50), ${}_i\boldsymbol{P}_{oc}$ and $[{}_i R_o^6]$ can be found directly as below:

$${}_i\boldsymbol{P}_{oc} = \begin{bmatrix} {}_i d_6 \, {}_i c_3 \, {}_i s_2 & {}_i d_2 - {}_i d_6 \, {}_i c_4 & {}_i d_1 - {}_i d_6 \, {}_i s_3 \, {}_i s_4 \end{bmatrix}^T \tag{51}$$

$$\begin{bmatrix} {}_i R_o^6 \end{bmatrix} = \begin{bmatrix} {}_i c_3 \, {}_i c_4 \, {}_i s_2 & {}_i s_3 \, {}_i c_5 - {}_i c_3 \, {}_i c_4 \, {}_i s_5 & {}_i c_3 \, {}_i s_5 \\ {}_i s_4 \, {}_i c_5 & -{}_i s_4 \, {}_i s_5 & -{}_i c_4 \\ -{}_i s_3 \, {}_i c_4 \, {}_i c_5 + {}_i c_3 \, {}_i s_5 & {}_i c_3 \, {}_i c_5 + {}_i s_3 \, {}_i c_4 \, {}_i s_5 & -{}_i s_3 \, {}_i s_4 \end{bmatrix}, \tag{52}$$

where ${}_i s_j = \sin {}_i\theta_j$ and ${}_i c_j = \cos {}_i\theta_j$. Note that the rotation matrix from the reference frame to the ith local base frame is written as

$$\begin{bmatrix} {}_i R_b^o \end{bmatrix} = Rot(\boldsymbol{z}_b, {}_i\gamma_b) = \begin{bmatrix} c_i\gamma_b & -s_i\gamma_b & 0 \\ s_i\gamma_b & c_i\gamma_b & 0 \\ 0 & 0 & 1 \end{bmatrix}, \quad i = 1, 2, 3, \tag{53}$$

and that the rotational matrix from the 6th local frame of the ith serial subchain to the output frame fixed to the platform is written as

$$\begin{bmatrix} {}_i R_6^p \end{bmatrix} = Robt(\boldsymbol{x}, -90^\circ) Rot(\boldsymbol{z}, {}_i\gamma_b) = \begin{bmatrix} c_i\gamma_p & -s_i\gamma_p & 0 \\ 0 & 0 & 1 \\ -s_i\gamma_p & -c_i\gamma_p & 0 \end{bmatrix}. \tag{54}$$

In eqs. (53) and (54), ${}_i\gamma_b$ and ${}_i\gamma_p$ represent the offset rotational angle about the axes $\boldsymbol{z}_b$ and $\boldsymbol{z}_p$, respectively. Therefore, the following equation holds:

$$\begin{bmatrix} {}_i R_b^p \end{bmatrix} = \begin{bmatrix} {}_i R_b^o \end{bmatrix} \begin{bmatrix} {}_i R_o^6 \end{bmatrix} \begin{bmatrix} {}_i R_6^p \end{bmatrix}. \tag{55}$$

Arranging eq. (55) with respect to $[{}_i R_o^6]$ gives

$$\begin{bmatrix} {}_i R_o^6 \end{bmatrix} = \begin{bmatrix} {}_i R_o^b \end{bmatrix} \begin{bmatrix} R_b^p \end{bmatrix} \begin{bmatrix} {}_i R_t^6 \end{bmatrix} = \begin{bmatrix} {}_i\boldsymbol{r}_{11} & {}_i\boldsymbol{r}_{12} & {}_i\boldsymbol{r}_{13} \\ {}_i\boldsymbol{r}_{21} & {}_i\boldsymbol{r}_{22} & {}_i\boldsymbol{r}_{23} \\ {}_i\boldsymbol{r}_{31} & {}_i\boldsymbol{r}_{32} & {}_i\boldsymbol{r}_{33} \end{bmatrix}. \tag{56}$$

From eqs. (53) and (56), $\theta_3, \theta_4, \theta_5$ can be found as follows:

$${}_i\theta_3 = a\tan 2(-{}_i r_{33}, {}_i r_{13}), \tag{57}$$

$${}_i\theta_4 = a\tan 2({}_i r_{13}/{}_i c_1, -{}_i r_{23}), \tag{58}$$

$${}_i\theta_5 = a\tan 2(-{}_i r_{22}, {}_i r_{21}). \tag{59}$$

It can be noted that since ${}_i\theta_3 \neq 0$ for real spherical joints, ${}_i\theta_4$ can always be obtained from eq. (58).

The output position vector can be written as

$$\boldsymbol{P}_c = \boldsymbol{P}_{bi} + {}_i\boldsymbol{P}_{oc}, \tag{60}$$

where

$$ {}_i\boldsymbol{P}_{oc} = \left[{}_i R_b^o\right]\{{}_i\boldsymbol{p}_{oc}\}. \tag{61} $$

Substituting eq. (52) into eq. (60) gives

$$ \boldsymbol{P}_c = \boldsymbol{P}_{bi} + \left[{}_i R_o^b\right]\begin{bmatrix} {}_i d_6 c_3 s_2 \\ {}_i d_2 - {}_i d_6 c_4 \\ {}_i d_1 - {}_i d_6 s_3 s_4 \end{bmatrix}. \tag{62} $$

Eq. (62) with respect to unknown input variables is arranged as below:

$$ \begin{bmatrix} {}_i d_6 c_3 s_2 \\ {}_i d_2 - {}_i d_6 c_4 \\ {}_i d_1 - {}_i d_6 s_3 s_4 \end{bmatrix} = \left[{}_i R_b^o\right]\begin{bmatrix} x - P_{ix} \\ y - P_{iy} \\ z - P_{iz} \end{bmatrix}. \tag{63} $$

Finally, from eqs. (53) and (63), desired input joint vectors can be found as

$$ {}_i d_6 = \frac{{}_i P_{ocx}}{{}_i c_1\ {}_i s_2}, \tag{64} $$

$$ {}_i d_2 = {}_i P_{ocy} + {}_i d_6\ {}_i c_4, \tag{65} $$

$$ {}_i d_1 = {}_i P_{ocz} + {}_i d_6\ {}_i s_3\ {}_i s_4. \tag{66} $$

3. Kinematic Characteristics of a 3-PPSP Mechanism

Define the output velocity vector as

$$ \dot{\boldsymbol{u}} = \begin{bmatrix} \dot{\boldsymbol{P}}_c^T & \boldsymbol{\omega}^T \end{bmatrix}^T, \tag{67} $$

where $\boldsymbol{\omega}$ represents the absolute angular velocity vector of the output frame. The forward-kinematic relationship between the output velocity vector and the input velocity vector can be found as follows (see appendix):

$$ \dot{\boldsymbol{u}} = [G_d^u]\dot{\boldsymbol{d}}. \tag{68} $$

Note that its reverse relationship can be expressed as

$$ \dot{\boldsymbol{d}} = [G_u^d]\dot{\boldsymbol{u}}. \tag{69} $$

To investigate kinematic characteristics of the mechanism, kinematic isotropic index defined by

$$ \sigma_{KI} = \frac{\sigma_{\min}([G_d^u])}{\sigma_{\max}([G_d^u])} \tag{70} $$

is used. In the simulation, it is assumed that the first active prismatic joint of each of serial subchain is placed perpendicularly to the base plate and symmetrically on the circle of radius of $R = 0.195$ located at the center of the base plate with an angle 120 degrees, and the second active prismatic joint is located perpendicularly to the first active prismatic joint as shown in Figure 2.

Figure 5(a)-(c) represents the contour plot of the isotropic index in the $x - y$ plane when $z = 0$, $\phi_{smax} = 90$ deg and the orientation of the platform is set to be (a) $\alpha = \beta = \gamma = 0$ deg, (b) $\alpha = 30$ deg, $\beta = \gamma = 0$ deg, (c) $\alpha = \beta = 0$ deg, $\gamma = 30$ deg, respectively, where ϕ_{smax} represents the maximum allowable displacements of spherical joints of the mechanism. It can be confirmed from these plots that the isotropic property of the mechanism is not affected significantly for the variation of the orientation of the platform.

Figure 6(a)-(c) represents the contour plot of the isotropic index in the $\alpha - \beta$ plane when $z = 0$, $\phi_{smax} = 90$ deg, and the output position and orientation of the platform is set to be (a) $x = y = 0$, $\gamma = 0$ deg, (b) $x = 0.1$, $y = 0$, $\gamma = 0$ deg, (c) $x = 0.1$, $y = 0$, $\gamma = 30$ deg. It can be seen from these plots that the parallel mechanism has the uniform kinematic characteristics around the center of its workspace.

4. Dynamic Characteristics of a 3-PPSP Mechanism

Note that the second-order kinematic relationships between output variables and the active input variables can be written as

$$ \ddot{\boldsymbol{d}} = [G_u^d]\ddot{\boldsymbol{u}} + \dot{\boldsymbol{u}}^T[H_{uu}^d]\dot{\boldsymbol{u}}, \tag{71} $$

and its reverse relationship can be written as

$$ \ddot{\boldsymbol{u}} = [G_d^u]\ddot{\boldsymbol{d}} + \dot{\boldsymbol{d}}^T[H_{dd}^u]\dot{\boldsymbol{d}}, \tag{72} $$

and that the dynamic equations for the mechanism with respect to active joint variables can be written as

$$ \boldsymbol{\tau}_d = [I_{dd}^*]\ddot{\boldsymbol{d}} + \dot{\boldsymbol{d}}^T[P_{ddd}^*]\dot{\boldsymbol{d}}, \tag{73} $$

where

$$ [I_{dd}^*] = [G_d^u]^T[I_{uu}^*][G_d^u], \tag{74} $$

$$ [P_{ddd}^*] = [G_d^u]^T\{[G_d^u]^T \circ [P_{uuu}^*] - [I_{dd}^*] \circ [H_{uu}^d]\}[G_d^u]. \tag{75} $$

Detailed derivations on eqs. (71) through (75) are given in the appendix.

Applying kinematic relationships between output variables and the active input variables, (69) and (71), to eq. (73) yields the dynamic equation between those two variables in the following form:

$$ \boldsymbol{\tau}_d = [I_{du}^*]\ddot{\boldsymbol{u}} + \dot{\boldsymbol{u}}^T[P_{duu}^*]\dot{\boldsymbol{u}}, \tag{76} $$

where

$$ [I_{du}^*] = [I_{dd}^*][G_u^d], \tag{77} $$

$$ [P_{duu}^*] = [G_u^d]^T[P_{ddd}^*][G_u^d] + [I_{dd}^*] \cdot [H_{uu}^d] \tag{78} $$

and

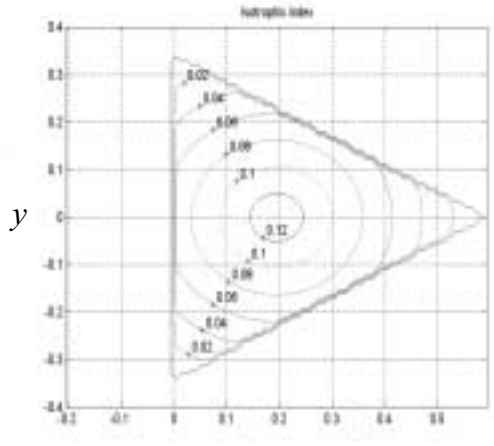

(a) $\alpha = \beta = \gamma = 0^{\circ}, P_{cz} = 0$

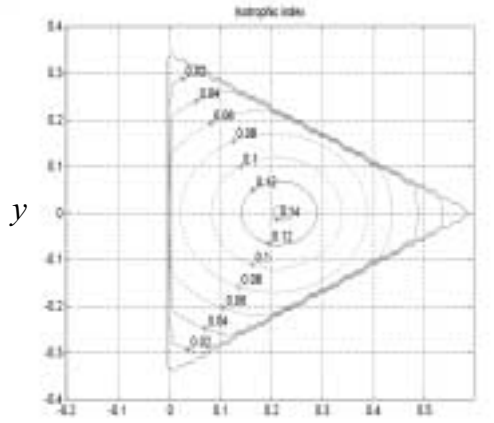

(b) $\alpha = 30^{\circ}, \beta = \gamma = 0^{\circ}, P_{cz} = 0$

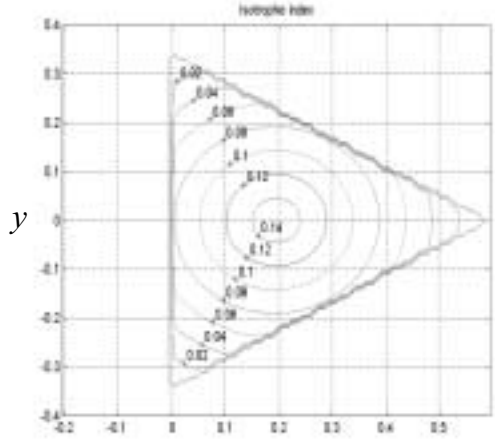

(c) $\alpha = \beta = 0^{\circ}, \gamma = 30^{\circ}, P_{cz} = 0$

Fig. 5. Contour plots of isotropic index in $x - y$ plane when $z = 0, \phi_{smax} = 90$ deg. (a) $\alpha = \beta = \gamma = 0°$, (b) $\alpha = 30°, \beta = \gamma = 0°$, (c) $\alpha = \beta = 0°, \gamma = 30°$.

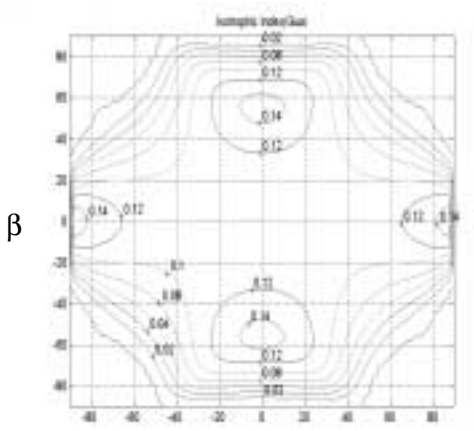

(a) $P_{cx} = 0.1, P_{cy} = P_{cz} = 0, \gamma = 0^{0}$

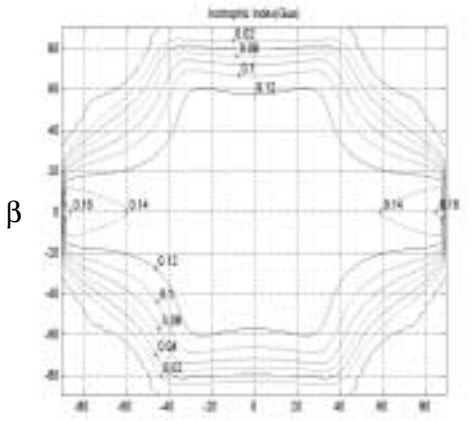

(b) $P_{cx} = P_{cy} = P_{cz} = 0, \gamma = 0^{0}$

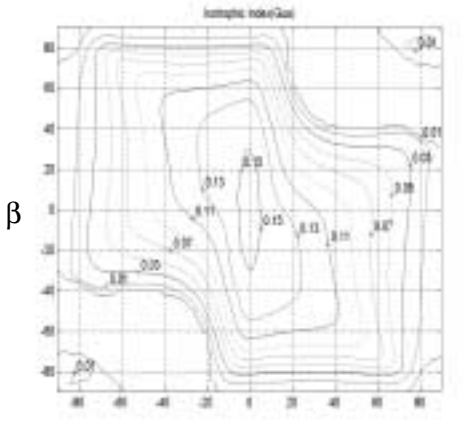

(c) $\gamma = 30^{0}, P_{cx} = 0.1, P_{cy} = P_{cz} = 0$

Fig. 6. Contour plots of isotropic index in $\alpha - \beta$ plane when $z = 0, \phi_{smax} = 90$ deg. (a) $x = y = 0, \gamma = 0°$, (b) $x = 0.1, y = 0, \gamma = 0°$, (c) $x = 0.1, y = 0, \gamma = 30°$.

$$[H_{uu}^d] = -[G_u^d]^T \left([G_u^d] \cdot [H_{dd}^u] \right) [G_u^d]. \tag{79}$$

In the above equations, $[I_{du}^*]$ represents the effective inertia matrix felt at active joints to produce the acceleration along the output direction of the mechanism when the manipulator is at rest.

Recently, Ma and Angeles (1993) proposed the dynamic design index representing the relationship between output acceleration and active input joint acceleration, that is, dynamic isotropic index defined as

$$\sigma_{DI} = \frac{\lambda_{\min}[I_{du}^*]}{\lambda_{\max}[I_{du}^*]}. \tag{80}$$

To investigate dynamic characteristics of the mechanism, the dynamic isotropic index is used in the following simulations.

Table 2 represents the estimated values of the link parameters of the implemented system and, in the following simulations, these values of the link parameters are used. Figure 7(a) represents the contour plot of the dynamic isotropic index of the parallel manipulator in the $x - y$ plane when the orientation of the top plate is set to $\alpha = \beta = \gamma = 0$ deg, $z = 0$, and $\phi_{smax} = 90$ deg. Figure 7(b) shows the contour plot of the dynamic isotropic index of the mechanism in the $\alpha - \beta$ plane when $z = R, x = y = 0, \gamma = 0$ deg and $\phi_{smax} = 90$ deg. It can be confirmed from these plots that dynamic isotropic characteristics are fairly uniform throughout the mechanism's workspace, except a region around the boundary of the workspace where the dynamic isotropic characteristics change rapidly. Noting that in a real system, the hardware limitations such as limited joint angles and stroke length exclude this region from the workspace of the mechanism, it can be said that the mechanism has an excellent dynamic characteristic throughout most of its workspaces.

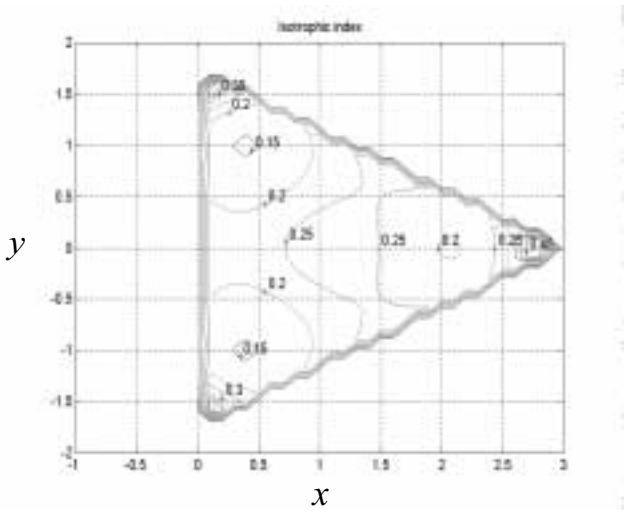

(a) $\alpha = \beta = \gamma = 0^0, P_{cz} = 0, \phi_{s\max} = 90^0$

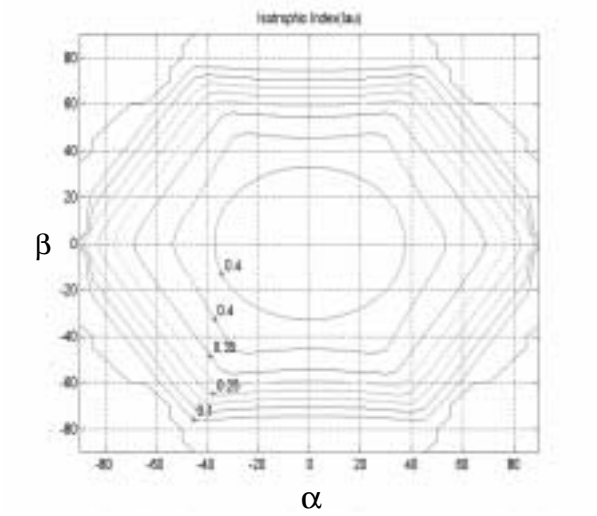

(b) $P_{cx} = P_{cy} = P_{cz} = 0,\ \gamma = 0^0, \phi_{s\max} = 90^0$

Fig. 7. Contour plots of isotropic index in $\alpha - \beta$, $x - y$ plane.

5. Implementation of the Parallel Mechanism

5.1. System Description

To test the performance of the 3-PPSP-type parallel mechanism, a prototype parallel manipulator system shown in Figure 8 is implemented. The implemented system hardware consists of a top plate and a base plate, three passive joints and six active prismatic joints, six DC servo-motors and servo-amplifiers, an AD converter with 32 channels, DA converters with 12 channels, DSP control boards, and a PC-586. The servo-controller used in this system is a DSP-based digital control system and its sampling rate is 2 kHz. As feedback position sensors, six rotary encoders and six limit sensors restricting the motion of the active prismatic actuators (i.e., its maximum stroke length is limited as 12 mm) are employed.

Table 2. Dynamic Parameters of a Parallel Manipulator

Link #n	m(Kg)	$P_{C_j}^{(j)}$(m)	$\Pi_{jk}^{(j)}$(Kg·m^2)
1	2.61	$[-0.015 \;\; 0 \;\; 0.02]^T$	
2	0.32	$[-0.01 \;\; 0 \;\; 0.02]^T$	
3	0	$[0 \;\; 0 \;\; 0]^T$	$I_{xy} = I_{yz} = I_{yz} = 0$ $I_{xx} = I_{yy} = I_{zz} = 0$
4	0	$[0 \;\; 0 \;\; 0]^T$	$I_{xy} = I_{yz} = I_{yz} = 0$ $I_{xx} = I_{yy} = I_{zz} = 0$
5	0.16	$[0 \;\; 0 \;\; 0.07]^T$	$I_{xx} = I_{yy} = 0.00030156$ $I_{zz} = 0.00000313$ $I_{xy} = I_{yz} = I_{yz} = 0$
6	0.14	$[0 \;\; 0 \;\; -0.1]^T$	$I_{xx} = 0.00003099$ $I_{yy} = 0.00003826$ $I_{zz} = 0.00003192$ $I_{xy} = I_{yz} = I_{yz} = 0$
Platform	1.537	$[0 \;\; 0 \;\; 0]^T$	$I_{xx} = I_{yy} = 0.00865382$ $I_{zz} = 0.01729125$ $I_{xy} = I_{yz} = I_{yz} = 0$

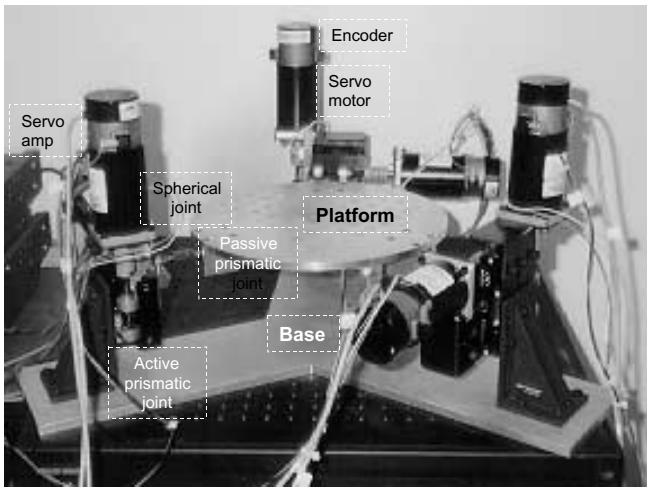

Fig. 8. The 6-DoF 3-PPSP prototype system.

5.2. Experiments on Movement of the Prototype Parallel Manipulator

The desired trajectory is selected: it starts from the origin of the reference frame and follows a spiral path until it reaches a circular path of radius 2.0 mm with its center at the z-axis in the $x - z$ plane without changing its output orientation. Then it follows the circular path with a frequency of 0.5 Hz. Figure 9(a) shows the plots from the trajectory-following experiments of the prototype mechanism for the given trajectory.

In this experiment, the joint-position servo-controller (PID control) provided by the DSP control boards is directly applied to the system. It is observed that the position servo-controlled prototype system shows relatively good trajectory-following capability. In Figure 9(b), the output position errors are computed by comparing the output position computed analytically from the forward-position analysis using the measured joint angular displacement data with the given trajectory. As can be seen in Figure 9(b), the system follows the given circular path with an error variation bound of 7 μm.

6. Conclusions

Closed-form forward/reverse-position solutions for a 3-PPSP 6-DoF parallel mechanism, which has some type of nonsymmetric geometry, are derived in this study. More specifically, the solution is valid to the mechanism that meets the following condition: three passive prismatic joints of each of three subchains are constrained to move parallel to the moving platform. Thus, the other system parameters of the mechanism do not need to be symmetric.

Kinematic and dynamic characteristics of the 3-PPSP mechanism are investigated via the isotropic index of the Jacobian matrix and of the output effective inertial matrix, respectively. From this study, it is found that the mechanism has fairly uniform kinematic/dynamic characteristics throughout its workspace.

To examine the effectiveness of the 3-PPSP-type mechanism, a prototype is implemented and joint-position servo-control is applied to the prototype system. From the experiments, it is shown that the controlled mechanism has a good trajectory-following performance. A more advanced controller requiring a forward- and/or reverse-position solution in real-time can be applied to the system to further enhance the performance of the mechanism by reducing both computational errors and computational burden.

As mentioned previously, the mechanism may not be adequate to tasks subject to high payloads. However, noting

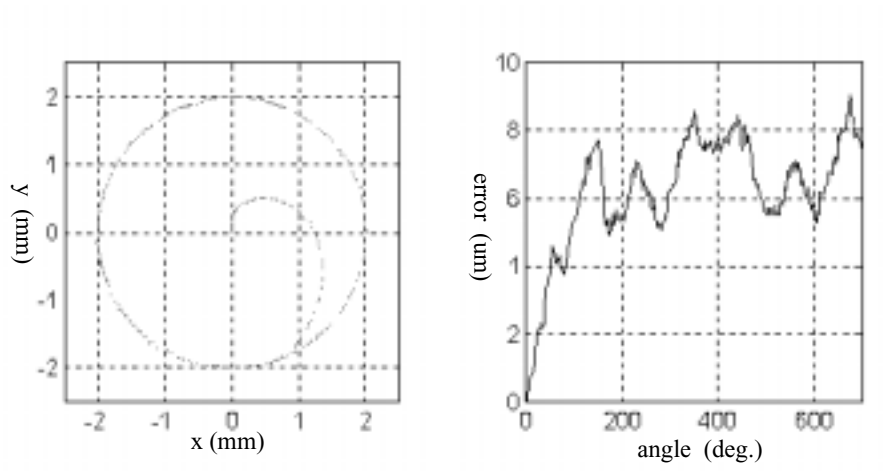

(a) circular motion (b) tracking error RMS

Fig. 9. Experimental results (PID control, circle motion in the $x - y$ plane). (a) Circular path and (b) error.

the above advantageous aspects, it can be contended that the mechanism can be effectively employed in tasks requiring high-precision and real-time operations.

Appendix

The following analysis is a summary on the modeling method proposed by Freeman and Tesar.

The First-Order Kinematic Model of a Serial Subchain

The Rotational First-Order Kinematic Influence Coefficient (KIC)

Denote ${}_i\boldsymbol{\omega}_j$ as the absolute angular velocity of the jth link of the ith serial subchain and ${}_i\boldsymbol{v}_j$ as the absolute translational velocity of a point of interest ${}_iP_j$ fixed on the jth link of the ith serial subchain. They are combined to form a vector ${}_i\dot{\boldsymbol{u}}_j$ representing the output linear/angular velocity vector of the jth link of the ith serial subchain as below:

$$ {}_i\dot{\boldsymbol{u}}_j = \begin{bmatrix} {}_i\boldsymbol{v}_j^T & {}_i\boldsymbol{\omega}_j^T \end{bmatrix}^T . \tag{A1} $$

Let ${}_i\dot{\boldsymbol{\phi}} = [{}_i\dot{\phi}_1 \quad {}_i\dot{\phi}_2 \quad \cdots \quad {}_i\dot{\phi}_N]^T$ be the joint velocity vector of the ith serial subchain. Then the relationship between ${}_i\boldsymbol{\omega}_j$ and ${}_i\dot{\boldsymbol{\phi}}$ can be expressed as

$$ {}_i\boldsymbol{\omega}_j = \begin{bmatrix} {}_iG_\phi^{jk} \end{bmatrix} {}_i\dot{\boldsymbol{\phi}}, \tag{A2} $$

where

$$ \begin{bmatrix} {}_iG_\phi^{jk} \end{bmatrix} = \begin{bmatrix} {}_i\boldsymbol{g}_{jk}^1 & {}_i\boldsymbol{g}_{jk}^2 & \cdots & {}_i\boldsymbol{g}_{jk}^N \end{bmatrix} \tag{A3} $$

and N represent the number of the joints in the ith serial subchain. Each column vector of the rotational first-order KIC, $[{}_iG_\phi^{jk}]$, is obtained as

$$ \boldsymbol{g}_{jk}^n = \begin{bmatrix} \boldsymbol{s}_n \text{ for } n \le j \text{ and } n = R \\ \boldsymbol{0} \text{ for } j > j \text{ and } n = P \end{bmatrix}, \tag{A4} $$

where $\boldsymbol{s}_n$ represents the unit vector along the direction in the nth joint axis, and R and P denote the revolute joint and the prismatic joint, respectively.

The Translational First-Order KIC

${}_i\boldsymbol{v}_j$ representing the absolute translational vector of an arbitrary point ${}_iP_j$ can be obtained as

$$ {}_i\boldsymbol{v}_j = [{}_iG_\phi^P]{}_i\dot{\boldsymbol{\phi}}, \tag{A5} $$

where

$$ [{}_iG_\phi^P] = \begin{bmatrix} {}_i\boldsymbol{g}_p^1 & {}_i\boldsymbol{g}_p^2 & \cdots & {}_i\boldsymbol{g}_p^N \end{bmatrix} \tag{A6} $$

and

$$ {}_i\boldsymbol{g}_p^n = \begin{cases} {}_i\boldsymbol{s}_n \times ({}_i\boldsymbol{P}_j - {}_i\boldsymbol{R}_n) \text{ for } n \le j \text{ and } n = R \\ {}_i\boldsymbol{s}_n \text{ for } n \le j \text{ and } n = P \\ \boldsymbol{0} \text{ for } n > j \text{ and } n = P. \end{cases} \tag{A7} $$

The matrix $[{}_iG_\phi^P]$ represents the translational first-order KIC for the point ${}_iP_j$. And ${}_i\boldsymbol{R}_j$ represents the absolute position vector to the origin of the jth local frame fixed to the jth link of the ith serial subchain from the origin of the reference frame.

From eqs. (A2) and (A5), the velocity relationship between output vector and input vector can be written as

$$\dot{\boldsymbol{u}} = [{}_iG_{\phi}^{u}]{}_i\dot{\boldsymbol{\phi}}, \tag{A8}$$

where

$$[{}_iG_{\phi}^{u}] = \begin{bmatrix} [{}_iG_{\phi}^{P}] \\ [{}_iG_{\phi}^{67}] \end{bmatrix} \tag{A9}$$

represents the Jacobian (the first-order KIC) of the ith serial subchain.

The First-Order KIC of the Parallel Mechanism

Assume that the number of the serial subchain of the parallel mechanism is L. When the Jacobian of each serial subchain is nonsingular, inverse relationship of eq. (A8) can be written as

$${}_i\dot{\boldsymbol{\phi}} = [{}_iG_{\phi}^{u}]^{-1}\dot{\boldsymbol{u}}, \quad \text{for } i = 1, 2, \ldots, L. \tag{A10}$$

Particularly for the 3-PPSP mechanism, the number of the serial subchain is 3 (i.e., $L = 3$) and it is assumed that the active input joint vector is defined as in (2). In this case, from eq. (A10), the relationship between active joint input velocity vector $\dot{\boldsymbol{d}}$ and the output velocity vector $\dot{\boldsymbol{u}}$ can be written as

$$\dot{\boldsymbol{d}} = [G_u^d]\dot{\boldsymbol{u}}, \tag{A11}$$

where

$$[G_u^d] = \Big[[{}_1G_{\phi}^{u}]_{1;}^{-T} \;\; [{}_1G_{\phi}^{u}]_{2;}^{-T} \;\; [{}_2G_{\phi}^{u}]_{1;}^{-T} \;\; [{}_2G_{\phi}^{u}]_{2;}^{-T} \;\; [{}_3G_{\phi}^{u}]_{1;}^{-T} \;\; [{}_3G_{\phi}^{u}]_{2;}^{-T} \Big]^T, \tag{A12}$$

and $[{}_iG_{\phi}^{u}]_{j;}^{-T}$ represents the transpose of the jth row vector of the matrix $[{}_iG_{\phi}^{u}]^{-1}$. Finally, the forward-kinematic relationship between the output velocity vector and the input velocity vector can be found by directly inverting eq. (A12) as follows:

$$\begin{aligned} \dot{\boldsymbol{u}} &= [G_u^d]^{-1}\dot{\boldsymbol{d}} \\ &= [G_d^u]\dot{\boldsymbol{d}}. \end{aligned} \tag{A13}$$

The Second-Order KIC of Serial Subchains

The Rotational Second-Order Kinematic Analysis

By differentiating eq. (A8) with respect to time, relationship between absolute angular acceleration vector of the jth link of the ith serial subchain and the input joint variable vector can be written as

$$\begin{aligned} {}_i\alpha_j &= \left[{}_iG_{\phi}^{jk}\right]{}_i\ddot{\boldsymbol{\phi}} + \left(\frac{d}{dt}\left[{}_iG_{\phi}^{jk}\right]\right){}_i\dot{\boldsymbol{\phi}} \\ &= \left[{}_iG_{\phi}^{jk}\right]{}_i\ddot{\boldsymbol{\phi}} + {}_i\dot{\boldsymbol{\phi}}^T\left[{}_iH_{\phi\phi}^{jk}\right]{}_i\dot{\boldsymbol{\phi}}, \end{aligned} \tag{A14}$$

where a three-dimensional array of $3 \times (N \times N)$, $[{}_iH_{\phi\phi}^{jk}]$, represents the second-order KIC of the jth link with respect to input joint variables and can be found as

$$\left[{}_iH_{\phi\phi}^{jk}\right]_{m;n} = \begin{bmatrix} {}_i\boldsymbol{s}_m \times {}_i\boldsymbol{s}_n & \text{for } m < n \le j \text{ and } m = R, n = R \\ \boldsymbol{0} & \text{otherwise} \end{bmatrix}. \tag{A15}$$

The Translational Second-Order Kinematic Analysis

The relationship between the translational acceleration vector of the point ${}_iP_j$ and the joint acceleration vector of the ith serial subchain can be obtained by direct differentiation of eq. (A11) with respect to time, as follows:

$$\begin{aligned} {}_i\ddot{\boldsymbol{a}}_j &= \left[{}_iG_{\phi}^{Pj}\right]{}_i\ddot{\boldsymbol{\phi}} + \left(\frac{d}{dt}\left[{}_iG_{\phi}^{Pj}\right]\right){}_i\dot{\boldsymbol{\phi}} \\ &= \left[{}_iG_{\phi}^{Pj}\right]{}_i\ddot{\boldsymbol{\phi}} + {}_i\dot{\boldsymbol{\phi}}^T\left[{}_iH_{\phi\phi}^{Pj}\right]{}_i\dot{\boldsymbol{\phi}}, \end{aligned} \tag{A16}$$

where $[{}_iH_{\phi\phi}^{Pj}]$ representing the translational second-order KIC can be found as follows:

$$\left[{}_iH_{\phi\phi}^{Pj}\right]_{m;n} = \begin{cases} {}_i\boldsymbol{s}_m \times [{}_i\boldsymbol{s}_n \times ({}_i\boldsymbol{P}_j - {}_i\boldsymbol{R}_n)] \\ \text{for } m \le n \le j \text{ and } m = R, n = R \\ {}_i\boldsymbol{s}_n \times [{}_i\boldsymbol{s}_m \times ({}_i\boldsymbol{P}_j - {}_i\boldsymbol{R}_m)] \\ \text{for } n \le m \le j \text{ and } m = R, n = R \\ {}_i\boldsymbol{s}_n \times {}_i\boldsymbol{s}_m \\ \text{for } n \le m \le j \text{ and } m = P, n = R \\ {}_i\boldsymbol{s}_m \times {}_i\boldsymbol{s}_n \\ \text{for } m \le n \le j \text{ and } m = R, n = P \\ \boldsymbol{0} \qquad \text{otherwise.} \end{cases} \tag{A17}$$

In (A17), ${}_i\boldsymbol{R}_n$ represents the absolute position vector from the origin of the reference frame to the origin of the nth local frame.

Similarly, the translational second KIC array, $[{}_iH_{\phi\phi}^{cj}]$, representing the relationship between the nonlinear acceleration of the mass center ${}_iP_{cj}$ of the jth link of the ith serial subchain and the joint acceleration of the ith serial subchain, can obtained from eq. (A17) by simply substituting ${}_i\boldsymbol{P}_{cj}$, representing the absolute position vector to the mass center of the jth link of the ith serial subchain, for ${}_i\boldsymbol{P}_j$, respectively. Particularly, it can be noted that for the 3-PPSP parallel mechanism, the position vectors representing the mass centers of the third and the fourth links can be approximated as

$${}_i\boldsymbol{P}_{c3} = {}_i\boldsymbol{R}_3, \tag{A18}$$

$${}_i\boldsymbol{P}_{c4} = {}_i\boldsymbol{R}_4. \tag{A19}$$

From (A14) and (A16) and assuming that the output vector of each of the serial subchains of the parallel mechanism is

assigned to have the same output vector $\boldsymbol{u}$, the relationship between the output acceleration and the input joint vector of the ith serial subchain can be obtained as

$$\ddot{\boldsymbol{u}} = [{}_iG^u_\phi]{}_i\ddot{\boldsymbol{\phi}} + {}_i\dot{\boldsymbol{\phi}}^T[{}_iH^u_{\phi\phi}]{}_i\dot{\boldsymbol{\phi}}, \tag{A20}$$

where

$$[{}_iH^u_{\phi\phi}] = \begin{bmatrix} [{}_iH^{Pj}_{\phi\phi}] \\ [{}_iH^{jk}_{\phi\phi}] \end{bmatrix} \tag{A21}$$

represents the second KIC of the jth link of the ith serial subchain with respect to the joints of the ith serial subchain.

The inverse relationship of eq. (A20) can be written as

$${}_i\ddot{\boldsymbol{\phi}} = [{}_iG^u_\phi]^{-1}\ddot{\boldsymbol{u}} + \dot{\boldsymbol{u}}^T[{}^iH^\phi_{uu}]\dot{\boldsymbol{u}}. \tag{A22}$$

From eq. (A22), the acceleration relationship between output variables and active input joint variables of the parallel mechanism can be expressed as

$$\ddot{\boldsymbol{d}} = [G^u_d]^{-1}\ddot{\boldsymbol{u}} + \dot{\boldsymbol{u}}^T[H^d_{uu}]\dot{\boldsymbol{u}}, \tag{A23}$$

where

$$[H^d_{uu}] = \begin{bmatrix} [{}_1H^\phi_{uu}]_{1;;} \\ [{}_1H^\phi_{uu}]_{2;;} \\ [{}_2H^\phi_{uu}]_{1;;} \\ [{}_2H^\phi_{uu}]_{2;;} \\ [{}_3H^\phi_{uu}]_{1;;} \\ [{}_3H^\phi_{uu}]_{2;;} \end{bmatrix}, \tag{A24}$$

and $[{}_iH^\phi_{uu}]_{j;;}$ represents the jth plane matrix of the three-dimensional array $[{}_iH^\phi_{uu}]$. Finally, substituting (A13) into (A23) and manipulating the result yields the acceleration relationship between the active joint input vector $\boldsymbol{d}$ and the output vector $\boldsymbol{u}$,

$$\ddot{\boldsymbol{u}} = [G^u_d]\ddot{\boldsymbol{d}} + \dot{\boldsymbol{d}}^T[H^u_{dd}]\dot{\boldsymbol{d}}, \tag{A25}$$

where

$$[H^u_{dd}] = -\left\{[G^u_d] \circ ([G^u_d]^T[H^u_{dd}][G^u_d])\right\}. \tag{A26}$$

In (A26), operator $\circ$ is called the generalized dot product and is defined as follows: let A and B represent a $p \times q$ matrix and a three-dimensional $q \times (m \times n)$ array. The resulting $p \times (m \times n)$ array C is obtained as

$$C_{pij} = [A \circ B]_{pij} = \sum_{k=1}^{q} A_{pk}B_{kij}. \tag{A27}$$

Dynamic Modeling of the 3-PPSP Parallel Mechanism

Dynamic Modeling of a Serial Subchain

Denote $[{}_i\Pi_{jk}]$ and $[\Pi^{(j)}_{jk}]$ as the global inertia matrix of the jth link of the ith serial subchain about its mass center and the local inertia matrix with respect to the local frame at the center of the jth link, respectively. They are related to each other as below:

$$[{}_i\Pi_{jk}] = [{}_iR^j_b][{}_i\Pi^{(j)}_{jk}][{}_iR^j_b]^T, \ j = 1, 2, \ldots, N. \tag{A28}$$

The dynamic equation of the ith serial subchain can be expressed as

$${}_i\boldsymbol{\tau}_\phi = [{}_iI^*_{\phi\phi}]{}_i\ddot{\boldsymbol{\phi}} + {}_i\dot{\boldsymbol{\phi}}^T[{}_iP^*_{\phi\phi\phi}]{}_i\dot{\boldsymbol{\phi}}, \tag{A29}$$

where $[{}_iI^*_{\phi\phi}]$ and $[{}_iP^*_{\phi\phi\phi}]$ represent the effective inertia matrix and the effective inertia power array with respect to joint variables, respectively, and they can be obtained as follows:

$$[{}_iI^*_{\phi\phi}] = \sum_{j=1}^{N}\{M_{jk}[{}_iG^{c_j}_\phi]^T[{}_iG^{c_j}_\phi] + [{}_iG^{jk}_\phi]^T[{}_i\Pi_{jk}][{}_iG^{jk}_\phi]\}, \tag{A30}$$

$$\begin{aligned}[{}_iP^*_{\phi\phi}] = \sum_{j=1}^{N}\{&M_{jk}\left([{}_iG^{c_j}_\phi]^T \circ [{}_iH^{c_j}_{\phi\phi}]\right) \\ &+ \left([{}_iG^{jk}_\phi]^T[{}_i\Pi_{jk}]\right) \circ [{}_iH^{jk}_{\phi\phi}] \\ &+ [{}_iG^{jk}_\phi]^T\left([{}_iG^{jk}_\phi]^T \circ [{}_iP_{jk}]\right)[{}_iG^{jk}_\phi]\},\end{aligned} \tag{A31}$$

where M_{jk} denotes the mass of the link j of the ith serial subchain.

Defining $[{}_i\Pi_{jk}]$ as

$$[{}_i\Pi_{jk}] = \begin{bmatrix} {}_iI_{jx} & {}_iI_{jy} & {}_iI_{jz} \end{bmatrix}, \tag{A32}$$

and using the relationship

$${}_i\boldsymbol{\omega}_{jk} \times [{}_i\Pi_{jk}]{}_i\boldsymbol{\omega}_{jk} = {}_i\boldsymbol{\omega}^T_{jk}[{}_iP_{jk}]{}_i\boldsymbol{\omega}_{jk}, \tag{A33}$$

the $[{}_iP_{jk}]$ in eq. (A30) can be found as

$$[{}_iP_{jk}] = \begin{bmatrix} [\boldsymbol{0}^T_{3\times1} & {}_i\boldsymbol{I}^T_{jz} & -{}_i\boldsymbol{I}^T_{jy}]^T \\ [-{}_i\boldsymbol{I}^T_{jz} & \boldsymbol{0}^T_{3\times1} & {}_i\boldsymbol{I}_{jx}]^T \\ [{}_i\boldsymbol{I}^T_{jy} & -{}_i\boldsymbol{I}^T_{jx} & \boldsymbol{0}_{3\times1}]^T \end{bmatrix}, \tag{A34}$$

where ${}_i\boldsymbol{\omega}_{jk}$ represents the absolute angular velocity.

Dynamic Model of the Parallel Mechanism

From the principle of the virtual work, the relationship between joint torques and output torques is expressed as

$${}_i\boldsymbol{\tau}_\phi \cdot \boldsymbol{\delta}_i\boldsymbol{\phi} = \boldsymbol{\tau}_u \cdot \boldsymbol{\delta u}. \tag{A35}$$

Using eq. (A11) and eq. (A35), the dynamic equation of the ith serial subchain in operational space is written as

$$ {}_i\boldsymbol{\tau}_u = [{}_i I^*_{\phi\phi}]\ddot{\boldsymbol{u}} + \dot{\boldsymbol{u}}^T [{}_i P^*_{uuu}]\dot{\boldsymbol{u}}, \tag{A36} $$

where

$$ [{}_i I^*_{uu}] = [{}_i G^{\phi}_u]^T [{}_i I^*_{uu}][{}_i G^{\phi}_u], \tag{A37} $$

$$ [{}_i P^*_{uuu}] = [{}_i G^{\phi}_u]^T \{[{}_i G^{\phi}_u]^T \circ [{}_i P^*_{\phi\phi\phi}] - [{}_i I^*_{uu}] \circ [{}_i H^u_{\phi\phi}]\}[{}_i G^{\phi}_u]. \tag{A38} $$

Therefore, the dynamic equation of the whole parallel mechanism in operational space is written as

$$ \boldsymbol{\tau}_u = [I^*_{uu}]\ddot{\boldsymbol{u}} + \dot{\boldsymbol{u}}^T [P^*_{uuu}]\dot{\boldsymbol{u}}, \tag{A39} $$

where

$$ [I^*_{uu}] = [I_{uu}] + \sum_{i=1}^{L} [{}_i I^*_{uu}], \tag{A40} $$

$$ [P^*_{uuu}] = [P_{uuu}] + \sum_{i=1}^{L} [{}_i P^*_{uuu}]. \tag{A41} $$

In eq. (A36), $[I_{uu}]$ and $[P_{uuu}]$ represent the local inertia matrix and the inertia modeling array of the remaining body, which are not included in the modeling of the serial subchain. When we denote the mass and the global inertia matrix of the body as M_p and $[\Pi_p]$, respectively, $[I_{uu}]$ and $[P_{uuu}]$ can be found as follows:

$$ [I_{uu}] = \begin{bmatrix} M_p[\boldsymbol{I}_{3\times3}] & [\boldsymbol{0}_{3\times3}] \\ [\boldsymbol{0}_{3\times3}] & [\Pi_p] \end{bmatrix}, \tag{A42} $$

$$ [P_{uuu}]_{1;:} = [P_{uuu}]_{2;:} = [P_{uuu}]_{3;:} = [\boldsymbol{0}_{6\times6}], \tag{A43} $$

$$ [P_{uuu}]_{4;:} = \begin{bmatrix} [\boldsymbol{0}_{3\times3}] & [\boldsymbol{0}_{3\times3}] \\ [\boldsymbol{0}_{3\times3}] & [\boldsymbol{0}^T_{3\times1} \;\; \boldsymbol{I}^T_{pz} - \boldsymbol{I}^T_{py}]^T \end{bmatrix}, \tag{A44} $$

$$ [P_{uuu}]_{5;:} = \begin{bmatrix} [\boldsymbol{0}_{3\times3}] & [\boldsymbol{0}_{3\times3}] \\ [\boldsymbol{0}_{3\times3}] & -[\boldsymbol{I}^T_{pz} \;\; \boldsymbol{0}^T_{3\times1} \;\; \boldsymbol{I}^T_{px}]^T \end{bmatrix}, \tag{A45} $$

$$ [P_{uuu}]_{6;:} = \begin{bmatrix} [\boldsymbol{0}_{3\times3}] & [\boldsymbol{0}_{3\times3}] \\ [\boldsymbol{0}_{3\times3}] & [\boldsymbol{I}^T_{py} - \boldsymbol{I}^T_{px} \;\; \boldsymbol{0}^T_{3\times1}]^T \end{bmatrix}, \tag{A46} $$

where $[\Pi_p]$ in eq. (A42) is denoted as

$$ [\Pi_p] = \begin{bmatrix} \boldsymbol{I}^T_{px} & \boldsymbol{I}^T_{py} & \boldsymbol{I}^T_{pz} \end{bmatrix}^T. \tag{A47} $$

Finally, using eq. (A39) and the principle of virtual work between the output vector and the active input vector, the dynamic equations of the mechanism with respect to active joint variables can be found as

$$ \boldsymbol{\tau}_d = [I^*_{dd}]\ddot{\boldsymbol{d}} + \dot{\boldsymbol{d}}^T [P^*_{ddd}]\boldsymbol{d}^*, \tag{A48} $$

where

$$ [I^*_{dd}] = [G^u_d]^T [I^*_{uu}][G^u_d], \tag{A49} $$

$$ [P^*_{ddd}] = [G^u_d]^T \{[G^u_d]^T \circ [P^*_{uuu}] - [I^*_{dd}] \circ [H^d_{uu}]\}[G^u_d]. \tag{A50} $$

References

Alizade, R. I., and Tagiyev, N. R. 1994. A forward and reverse displacement analysis of a in-parallel manipulator. *Mechanism and Machine Theory* 29(1):115–124.

Behi, F. 1988. Kinematic analysis for a six-degree-of-freedom 3-PRPS parallel mechanism. *IEEE Journal of Robotics and Automation* 4(5):324–331.

Byun, Y. K., and Cho, H. S. 1997. Analysis of a novel six-degree-of-freedom 3-PPSP parallel manipulator. *Journal of Robotics Research* 16(6):612–618.

Byun, Y. K., Cho, H. S., Kim, W. K., Baek, S. E., Chang, H. S., and Rho, K. C., 1998. Kinematic/dynamic analysis of a 6 DOF parallel manipulator with 3-PPSP serial subchains and its implementation. *'98 IROS Conf.*, Victoria, B. C., Canada, pp. 1981–1986.

Cleary, K., and Brooks, T. 1993. Kinematic analysis of a novel 6-DOF parallel manipulator. *Proc. IEEE Intl. Conf. on Robotics and Automation* 2:708–713.

Freeman, R. A., and Tesar, D. 1988. Dynamic modeling of serial and parallel mechanisms/Robotic systems, Part I—Methodology, Part II—Applications, *20th Biennial Mech. Conf.*, Kissimme, FL, pp. 7–27.

Hudgens, J., and Tesar, D. 1991. Analysis of a fully-parallel 6-DOF micromanipulator. *Proc. IEEE Intl. Conf. on Robotics and Automation* 2:814–820.

Kohli, D., and Lee, S. H. 1988. Manipulator configurations based on rotary-linear (R-L) actuators and their direct and inverse kinematics. *Journal of Mech. Trans. and Auto. Design* 110:397–404.

Ma, O., and Angeles, J. 1993. Optimum design of manipulators under dynamic isotropy conditions. *Proc. IEEE Intl. Conf. on Robotics and Automation* 1:470–475.

Merlet, J. P. 1993. Closed-form resolution of the direct kinematics of parallel manipulator using extra sensors data. *Proc. IEEE Intl. Conf. on Robotics and Automation* 1:200–204.

Tsai, L. W., and Tahmasobi, F. 1993. Synthesis and analysis of a new class of six degree-of-freedom parallel manipulators. *Journal of Robotic Systems* 10(5):561–580.